Proceedings of IMECE 2003:
International Mechanical Engineering Congress and Exhibition
November 16-21, 2003 in Washington, DC

IMECE2003-41388

A BATCH FABRICATED LINEAR SYNCHRONOUS MOTOR

Martin Föhse
Institute for Microtechnology,
Hanover University,
Callinstraße 30A, D-30167 Hanover, Germany

Jens Edler
Institute for Drive Systems and Power Electronics
Hanover University,
Welfengarten 1, D-30167 Hanover, Germany

Hans-D. Stölting
Institute for Drive Systems and Power Electronics
Hanover University,
Welfengarten 1, D-30167 Hanover, Germany

Hans H. Gatzen
Institute for Microtechnology
Hanover University,
Callinstraße 30A, D-30167 Hanover, Germany

ABSTRACT

Micro electro-mechanical systems (MEMS) technology opens up new ways of miniaturizing electromagnetic motors. A very promising approach for building miniature linear actuators is to fabricate the stator as well as the traveler separately and merging the motor components in a microassembly process [1]. This paper describes design, fabrication, and evaluation results of a linear synchronous actuator following this basic approach.

INTRODUCTION

For microactuators, the electromagnetic drive scheme has several advantages compared to others like electrostatic or piezoelectric. Electromagnetic actuators allow for a rather high energy density [2] resulting in a suitable torque for rotating motors or driving force for linear actuators, respectively. At the same time these micromotors exhibit a robust design and are relatively insensitive to pollution in the micro range. Last but not least, one can draw on vast experiences with the design and optimization of larger machines with the electromagnetic drive scheme. Mostly the respective knowledge as well as the design and calculation tools are easily transferable to micromotors.

For positioning applications, linear motor designs are superior to the rotational ones. Such motors do not require any gear boxes [3], thus substantially reducing design complexity. While the cost of fabrication decrease, the positioning accuracy does increase due to smaller tolerances of the actuator's mechanical structure. Compared to other linear drives, the design of electromagnetic actuators can be easily adopted to a continuos motion that is mainly limited by the bearing and traveler dimensions.

One of the main advantages of electromagnetic actuators is the variety of motor types available, like variable reluctance (VR) stepping motors, hybrid stepping motors, asynchronous, electronically commutated (EC), and synchronous motors. Nevertheless the most explored actuators are those with the VR drive scheme [1, 4, 5, 6]. This is due to their simple design with only three functional materials: soft magnetic material for the flux guides, conductive material for the coil system, and insulators for insulating the coil turns. Furthermore, VR-motors fit for positioning applications since these motors include a serrated magnetic air gap.

On the other hand, motors with additional integrated hard magnets allow for a much higher driving force and an even more robust design due to an increased air gap [7]. Possibly, electromagnetic motors with hard magnets like hybrid, synchronous, or EC actuators are suitable for opening a wide field of applications for micromachined drive systems.

NOMENCLATURE

Electromagnetic microactuator, linear synchronous motor, hard magnets, linear bearing

DRIVE SCHEME

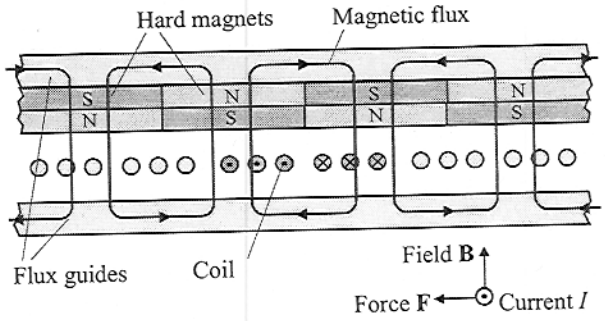

Figure 1: Synchronous drive scheme

Figure 1 depicts the main elements of a permanent magnet synchronous motor. In general, these motors use permanent

magnets to create a strong magnetic field **B** in the air gap, which interacts with the much weaker magnetic field created by the excited coils [8]. This results in a driving force **F** between the permanent magnets and coil described by Laplace's law

$$\mathbf{F} = I(\mathbf{l} \times \mathbf{B}), \quad (1)$$

with the current I, the conductor length **l** and the air gap flux density **B**. By applying a soft magnetic flux guide in the back of the hard magnets, the coils, or both of them, the magnetic circuit's reluctance can be significantly decreased. Therefore, the flux in the air gap is increased and the driving force increases, too.

Usually, synchronous motors are driven with a rotational (i.e. three phase) current system [8]. To allow for an adoption of this drive scheme, the new micromotor was designed with a three phase coil system, too. Figure 2 explains the motor's stepping mode in case of a step by step excitation of the phases.

In a first step, a current is applied to phase 1 that creates a north pole in the air gap. A south pole of the hard magnets aligns to this phase. Next, phase 2 is energized, creating a south pole at the air gap that attracts a north pole of the hard magnets. Not shown is the third step when phase 3, which is driven the same way as phase 1 in the first step (north pole in the air gap attracts a hard magnet's south pole). The second triplet of steps starts out again with phase 1, only now all polarities are reversed. After performing six steps, the sequence will start from the beginning.

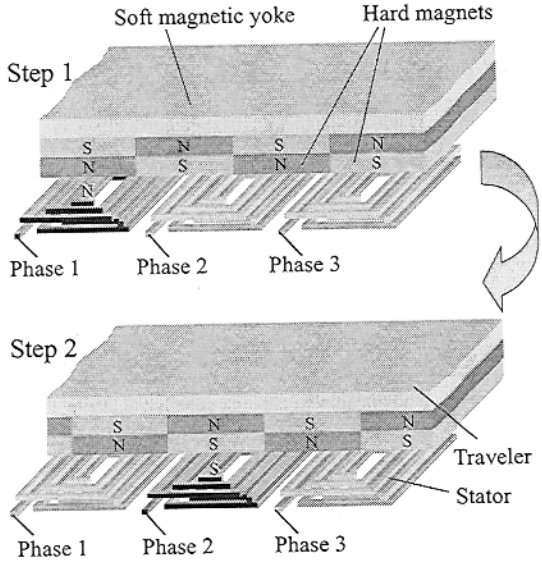

Figure 2: Stepwise movement of a synchronous motor (only two of six steps are shown)

Contrary to the described scheme usually two of the three phases are excited at any time to maximize the driving force. Driving the motor that way represents the full step mode. An improved positioning can be achieved when the motor is driven in the half step or even in the microstep mode. The half step mode is realized by switching off one phase in between every full step. By doing so, the half step mode doubles both the number of steps, as well as the positional accuracy.

In the microstep mode, additionally the current values of the phases are varied individually. Therefore, any position in between the full step positions can be obtained. Such an approach requires a positional feedback system. What positional accuracy may be achieved depends both on this feedback system, but also on the bearing behavior, like stick slip effects.

The stepping mode is reached when the motor is not driven by a sinusoidal three phase current but with a rectangular current profile. For testing the investigated synchronous micromotor the full step mode was realized by exciting only phase at each time (Fig. 3). This driving scheme was chosen for the microactuator described here.

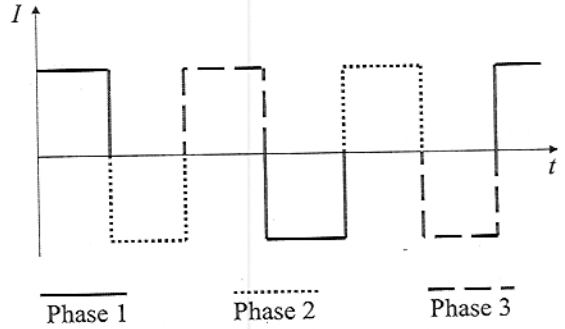

Figure 3: Sequence of phase excitation: rectangular current wave form

DESIGN

Stator

Principally, either the stator or the traveler may be equipped with coils, while the opponent may contain the hard magnets. However, to avoid electrical connections to the traveler, the coil system should be placed into the stator. Particularly in microactuators, either brushes or wire connections would hinder the traveler's motion significantly because of fiction or stiffness of the wire loop.

The stator of the linear synchronous micromotor was designed with three phases, each one represented by three double layer spiral coils.

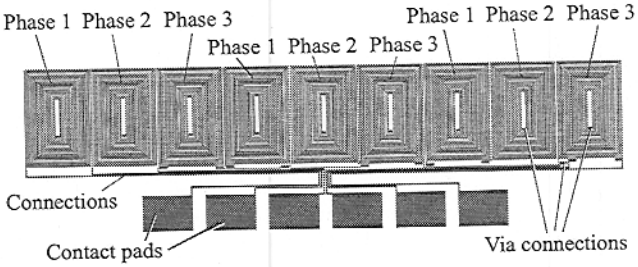

Figure 4: Layout design of the stator's first coil layer

Figure 4 depicts the design of the first coil layer. In the center of each of the nine coils, the via connection is located for contacting the second coil layer. All necessary connections for interconnecting the three coils of each phase with one another were included in the mask design. This allowed a simplification of contacting the stator system and a limitation of the number of contact pads to six. The size of the contact pads was chosen rather large and arranged in the usual 1/10 inch (2.54 mm) grid

to allow for flexible contacting techniques including soldering the wires.

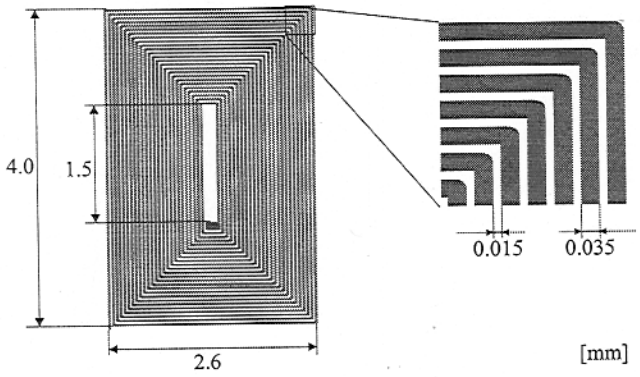

Figure 5: Single coil with detailed view of layer width

Each of the nine coils has 50 windings distributed in two layers. The lateral dimensions of the coils are shown in figure 5. The coil width is 35 µm and the gap between each other is 15 µm. With the physical dimensions chosen the coil length for each phase resulted in appr. 1,200 mm, thus promising a rather high system impedance.

Bearing and Traveler

The main disadvantage of electromagnetic linear actuators is the high normal force F_z caused by the electromagnetic attraction between stator and traveler. This attractive force directly influences the friction force F_f, connected by the coefficient of friction μ_r:

$$F_f = \mu_r \cdot F_z \overset{!}{<} F_x \qquad (2)$$

Therefore, a linear electromagnetic actuator requires generally a bearing system with a rather low coefficient of friction μ_r. A promising approach in reaching a small frictional value is to apply a micro ball bearing which had been developed previously [9, 10].

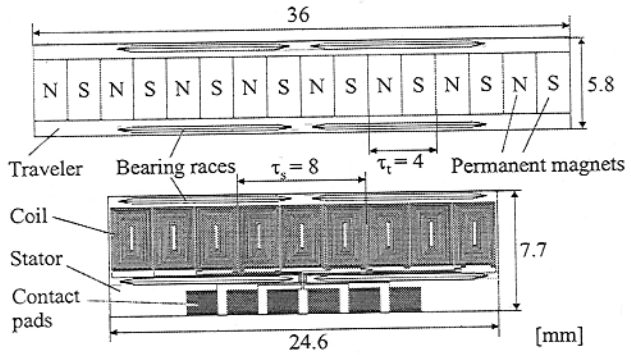

Figure 6: Lateral dimensions of the linear synchronous micromotor with ball bearing

This bearing takes advantage of high precision ruby balls (∅ 200 µm) running in mechanically micromachined V-grooves of great smoothness for races. With these micro ball bearings, a coefficient of friction μ_r of less than 0.01 could be achieved [10]. Contrary to the application of the micro ball bearings described in [10], for the synchronous micromotor both the stator and traveler were equipped with integrated V-grooves on the substrates consisting of two separated bearing races on both sides of the active part (Fig. 6).

In the stator, the bearing races are located on both sides of the active part and, on the contact side, between the active part and the contact pads. The hybrid hard magnets of the traveler were countersunk in special grooves of the traveler substrate and bonded. The lateral dimensions of the perpendicular magnetized permanent magnets are 2 x 3 mm with a thickness of 200 µm. Figure 6 depicts the overall dimensions of both, stator and traveler. With these data the traveler's displacement amounts to app. 11 mm.

CALCULATIONS

Calculations were applied to forces taking effect on the traveler, in particular the driving force F_x and the normal force F_z created by electromagnetics. This required fundamentally the knowledge of the magnetic field distribution in the air gap excited by the permanent magnets as well as of the distribution of the electric loading. In order to comply with this demand, the air gap field was determined by using a 3D finite element analysis (FEA) formulation in the field of one pole pitch. That way the field distortion caused by the large air gap related to the small pole pitch, the small extend of the motor crosswise to the direction of motion and the groove serving to fix the permanent magnets on the traveler could be considered.

The arrangement of permanent magnets and stator winding is shown in Fig. 1. The magnetic field strength excited by the winding is small compared to the field caused by the hard magnets. Therefore, a field distortion which is always caused by the electric loading of the stator winding, the so-called "armature reaction", was not taken into account calculating the motor's driving force.

The results presented here based on the magnetic field in the air gap in the winding layer. The motors driving force results from applying the Laplace's law (1), the normal force substantial caused by tensile stress acting on the stators soft magnetic yoke results from the Maxwell's force tensor:

$$\mathrm{d}\mathbf{F} = -\frac{\mu_0}{2} H^2 \,\mathrm{ds} + \mu_0 (\mathbf{H}\,\mathrm{ds})\,\mathbf{H} \qquad (3)$$

In the stepwise driving mode described above, only one phase is excited. The following results are based on this fact. Taking the air gap as the parameter results in the typical force-position-characteristics presented in Fig. 7 in the dimension of one pole pitch. The constant electric loading is about 5 ampere turns (I = 100 mA).

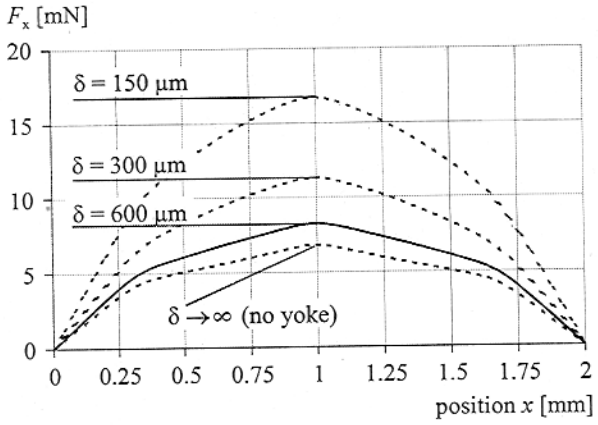

Figure 7: Typical force-position characteristics as a function of the air gap dimension

The diagram shows clearly that by using a soft magnetic yoke the driving force of the motor increases. This is caused by the enlarged magnetic flux density created by the permanent magnets. Without any yoke in stator the driving force decreases of app. 20 percent with reference to the values at an air gap of 600 µm.

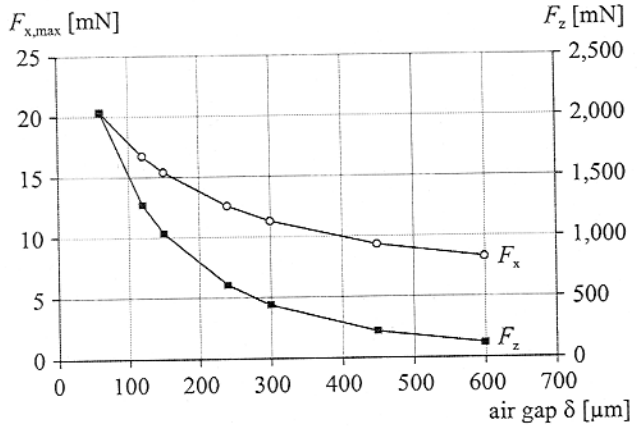

Figure 8: Driving force F_x and normal force F_z as a function of the air gap dimension

But the Maxwell forces take a negative effect on the driving force because friction become more and more important. Figure 8 depicts the dependence of F_x and F_z on the air gap. The normal force increases much more than the driving force. The conclusion is that choosing the minimal air gap at a constant electric loading have to be done carefully. This is a very important aspect in the design of linear motors, particularly in micro linear motors.

FABRICATION

Thinfilm Fabrication of the Stator

The thinfilm fabrication of the stator started out with the sputter deposition of a copper seed layer on the isolated substrate. As wafer materials for stator either silicon or MnZn-ferrite were applied; the wafers used were 4 in round. Contrary to silicon, ferrite substrates represent an additional flux guide for the stator and by this, minimize the reluctance of the magnetic circuit. On the other hand, this approach results in a significantly strengthened magnetic field which increases the normal force even without excitation of the coils. In the case of silicon wafers, a compromise was found by adding a steel sheet on the wafer backside as a soft magnetic yoke.

Insulation between the seed layer and the substrate is accomplished by thermal oxidization of the silicon or sputter deposition of an alumina layer in case of a ferrite wafer. Figure 9 shows the main fabrication steps for fabricating the double layer spiral coils for the electromagnetic field excitation.

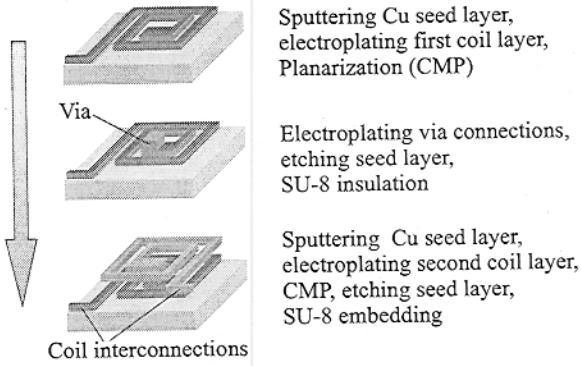

Figure 9: Thinfilm fabrication steps for the stator

Photolithography of the coil layers as well as of the via connection was done with DNQ/Novolac resist (AZ9260, Clariant). Electroplating utilizing a sulfate based copper electrolyte was applied for depositing all coil and via structures. Due to field distortion, the coil's film thickness varied from 20 to 40 µm. Therefore, after deposition of the coil layers a planarization step was necessary to reach an uniform coil cross section of nominal 35 µm width and 20 µm height. It is accomplished by a chemical mechanical polishing (CMP) process similar to the one reported in [11]. After treating the first coil layer as described above, another lithography and electroplating step was utilized to create all via connections. Next, the seed layer was removed by ion beam etching (IBE).

An insulation between the first and second coil layer was accomplished by patterning a photosensitive epoxy (Epon SU-8). This resist achieves a high degree of planarization (DOP) [12] and is well suited for embedding the high aspect ratio copper coils. After depositing another seed layer and applying photolithography as well as electroplating of copper for the second coil layer, these structures had to be also planarized. Finally, the whole coil system was embedded in SU-8 for protecting the copper against oxidization.

Fabrication Results

Before the stator systems (25 on a 4 inch wafer) were diced, the bearing races were ground in the wafer surface. To do so, a profile dicing process with V-shaped dicing wheels described in [9] was applied. By cutting the grooves, a very high lateral precision of the bearing races could be reached. The lateral positioning accuracy was better than 200 nm, while the depth tolerance was 1 µm. Figure 10 depicts a completed and diced stator, fabricated on a ferrite substrate.

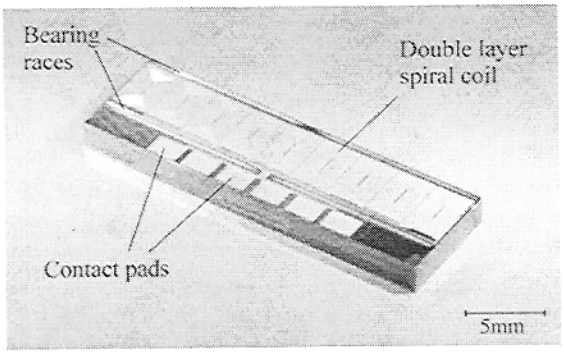

Figure 10: Completed stator on ferrite substrate

The feasibility of the fabrication process could be proven. A yield of 70 percent good parts per wafer could be achieved during prototype production. Figure 11 depicts one of the nine coils. At both sides of the photograph, there are bearing races with ruby balls. At the left side are interconnections and vias.

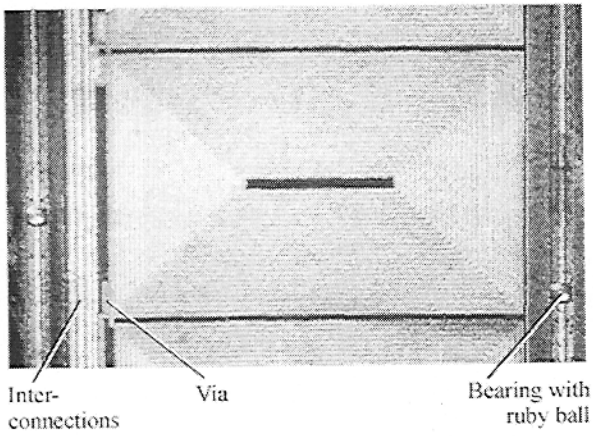

Figure 11: One double layer spiral coil (left) and detailed view of via connections (right)

Hybrid Traveler Fabrication and Assembly

As substrate for fabricating the traveler, a soft magnetic MnZn-ferrite (H3F5 by Sumitomo) was used. Table 1 lists the main magnetic properties of this material. Especially its rather high saturation flux density B_s of 570 mT qualifies this ferrite as a suitable flux guiding material.

Table 1: Magnetic properties of MnZn-ferrite

Saturation flux density B_s [mT]	570
Coercivity H_c [A/m]	18
Permeability μ_r	4,000

Fabrication of the traveler started with profile grinding the bearing races and dicing the traveler itself. For permanent magnets, a compound based on a NdFeB powder was used. Since water was used as a coolant for the dicing process, the highly corrosive permanent magnets were mounted after the separation process. Table 2 lists the key properties of the permanent magnetic material (Vacophan 3.5, Vacuumschmelze).

Table 2: Magnetic properties of NdFeB

Saturation flux density B_s [mT] @ 20°C	600
Remanence flux density B_r [mT] @ 20°C	410
Coercivity H_c [kA/m] @ 20°C	800
Energy product BH_{max} [kJ/m³] @ 20°C	28

For optimizing the efficiency of the micromotor, the length of air gap between stator and traveler had to be minimized. In contrast to the stator, where the structure thickness is defined by thinfilm fabrication and CMP for the traveler, the accuracy of the air gap width is defined by the mounting tolerances of the permanent magnets. Therefore, a bonding groove was ground into the ferrite substrate that served as a reservoir for the epoxy adhesive (Fig 12). This way, a lifting of the permanent magnets due to creeping of the epoxy caused by capillary action could be prevented.

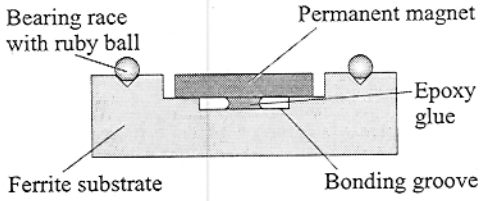

Figure 12: Bonding principle for hybrid mounting (cross section of the traveler)

MEASUREMENTS

Electrical Characterization

Figure 13 demonstrates the electrical behavior of the linear synchronous micromotor as a function of the driving frequency. It shows the typical characteristic of an electromagnetic coil interacting with a soft magnetic yoke of finite magnetic conductivity. While the real part of the impedance $\Re\{\underline{Z}\}$ increases with the measuring frequency f, the inductance L decreases.

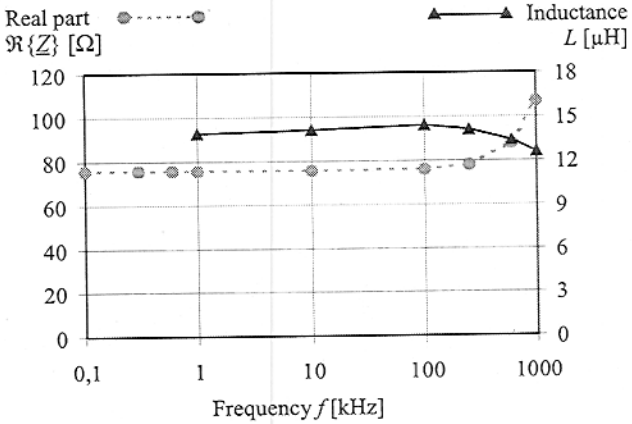

Figure 13: Single phase resistance and inductance measurements

For low frequencies f $\Re\{\underline{Z}\}$ of one phase was app. 75 Ω, while the inductance L was 14 µH. Therefore, the electrical characteristic quantity of the coil system can be assumed to be constant for driving frequencies with practical meaning below

100 kHz. Only at higher frequency values the measurements showed a significant changing of the coil parameters.

Measurements regarding the temperature for an excitation current of 100 mA (equal to a power dissipation of 0.75 W) showed a temperature rise of approximately 35 K (above room temperature RT). This amount of heating up is acceptable and does not result in an undue thermal distortion of the hybrid actuator. The temperature was determined by measuring the resistance R_T of a non-excited phase (with R_0 at RT). Assuming a constant heating of the whole system and using a known temperature resistance coefficient α [13], the heating ΔT could be calculated by using the following equation:

$$\Delta T = \frac{1}{\alpha}\left(\frac{R_T}{R_0} - 1\right) \qquad (4)$$

Force Measurement

For measuring the motor's force, an experimental setup was used that is shown schematically in Fig. 14. The synchronous micromotor was mounted on a positioning table moved by a micrometer screw. Force measurement was conducted with a precision glass beam used as a leaf spring and an optical determination of the beam deflection [14]. For a measurement, one phase of the motor was excited with a current I of 100 mA.

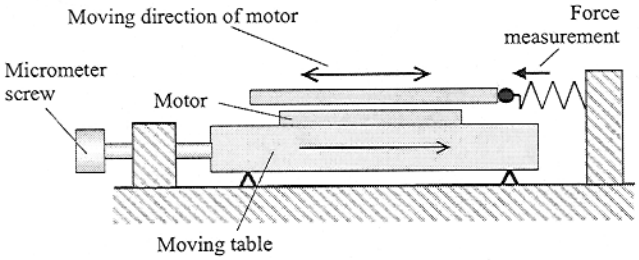

Figure 14: Force measurement schematics

With the described arrangement two springs are working against each other. The electromagnetic force aligning the permanent magnet pole of the traveler and the excited coil of the stator represents the first spring. This attractive force depends on the traveler's position relative to the stator and shows a spring like behavior. The second spring is the glass beam the micromotor pushes against.

For each measurement, the desired relative position between stator and traveler is achieved by adjusting the micrometer screw accordingly. This is done as follows: Before starting a measurement, the stator was excited and the traveler was moved in contact to the glass beam by actuating the positioning table accordingly. Figure 15 depicts a characteristic plot of these force measurements and compares them to the simulation results. In average, the simulation results are 20 percent greater than the actual experimental measurement values, which represents an excellent correlation.

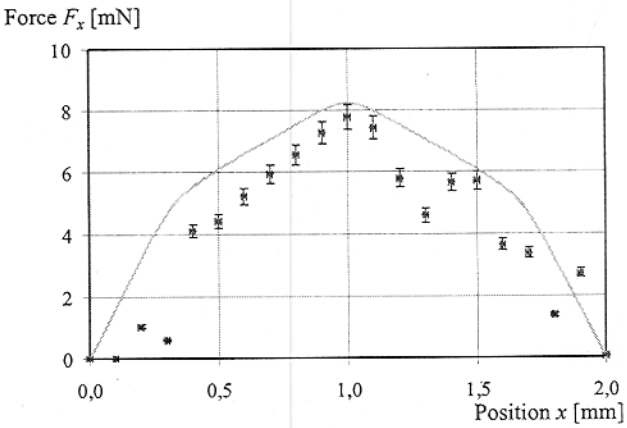

Figure 15: Comparison of simulation (solid line) and experimental results of the driving force

The force F_x increases from zero to a maximum of app. 8 mN, and then decreases again until the force reaches zero. At the center of the curve (at x=1 mm), the polarity seen by the coil's center changed from north to south pole (each permanent magnet is 2 mm wide). Therefore, the resulting force reached its maximum value.

A displacement of more than 1 mm caused the attraction force to decrease more and more. For a movement x of a total of 2 mm, the driving forces on the coil are opposite to each other and the resulting force becomes zero again.

The irregular increase and decrease of the curve was caused by stick slip in the bearing races. The route cause were irregularities in the groove surface, caused by the profile grinding process. This issue could be resolved by an optimization of the grinding process as well as by a change to silicon.

Positioning Accuracy

For determining the displacement of the traveler when different phases were excited, a laser triangulation system (Optocondt ILD 1800-2100) was utilized. The laser dot of the optical system was pointed at the reflective face of the traveler in driving direction. Figure 16 shows the experimental setup. With this arrangement, a sufficient resolution of app. one micron could be achieved.

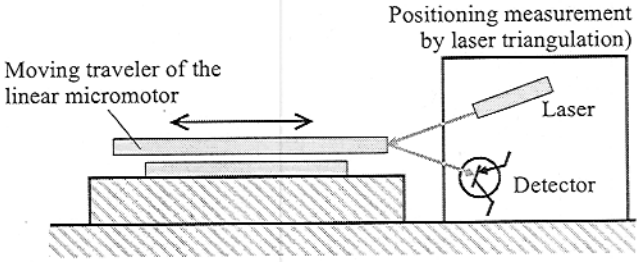

Figure 16: Positioning measurement schematics

One point of interest regarding positioning drive systems is their repeating accuracy. It could be determined by alternately exciting two phases of the synchronous micromotor, thus approaching the end position from either side. Figure 17 depicts a typical result of a repeating accuracy measurement. The

maximal deviation was 5 µm. These deviations were caused by bearing friction, but also by an overshooting of the traveler. This overshooting behavior increased when rather high excitation currents were applied. Therefore, the traveler sometimes got stuck in positions that otherwise were not taken.

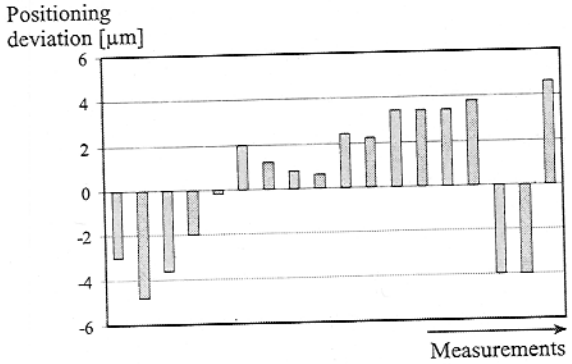

Figure 17: Experimental repeating accuracy results for phase 1 (sequence of 18 tests)

Figure 18 shows a damped oscillation of the traveler with the motor driven in half step mode and a current of 100 mA. The natural frequency of the mechanical system is appr. 19.7 Hz. The plot in Figure 18 may serve as a basis for an electronically regulated controlling. Even with the improved bearing surface, the accuracy obviously is limited by mechanical inaccuracy in the range of microns.

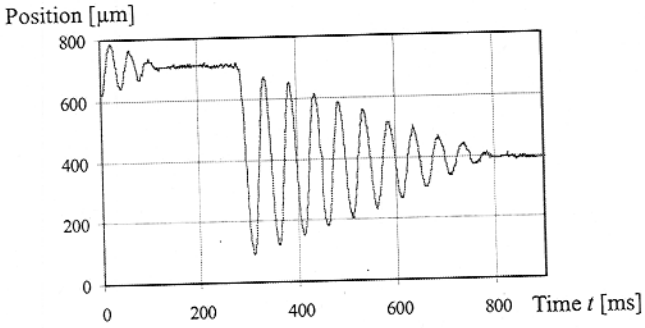

Figure 18: Damped oscillation measurement

The measurement setup was also used to determine the accuracy of the linear synchronous micromotor when driven in the microstep mode. To do so, two phases of the stator were excited with two different currents (I_1 and I_2). The maximal value for each phase current was 100 mA. While increasing one phase current starting with zero the other current was decreased by the same difference. Figure 19 depicts the traveler position dependent on the current difference ΔI (=I_1 - I_2).

Due to stick slip in the bearing races, the measured positions differed from the theoretical linear relationship in Figure 19. With a silicon stator and the groves machined by an improved profile grinding process, a maximal positional accuracy of app.1 µm could be achieved.

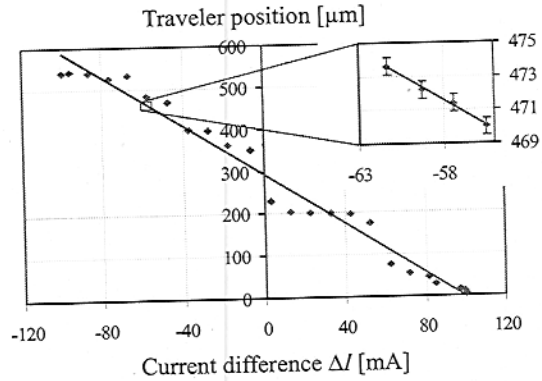

Figure 19: Positioning accuracy measurement

SUMMARY AND OUTLOOK

It could be shown that a hybrid approach provides a very promising path for fabricating a MEMS type synchronous linear micromotor. The feasibility of the fabrication process could be proven, the wafer level yield during prototype production was 70%.

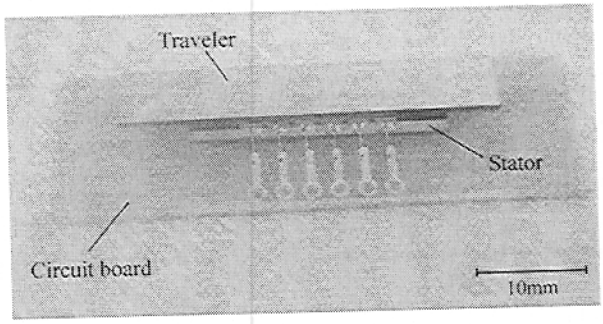

Figure 20: Complete synchronous micromotor assembly

The synchronous micromotor features a total travel of 11 mm, a positioning accuracy in the micron range, and a maximal driving force of 10 mN. The calculation tools for designing the motor proved their capability by predicting results which in average deviated from experimental data by only 20 percent.

Future activities on the synchronous micromotor will focus mainly on a batch fabrication of the traveler. To do so, a thinfilm fabrication of the permanent magnets will be required. The Institute for Microtechnology developed a sputtering process for depositing rather thick SmCo films [15] which will be applied for this process. However, the successful use of thinfilm permanent magnets in microactuators will also depend on coming up with a process for an in situ magnetization of the permanent magnets.

An other venue of activities will be to extend the synchronous micro drive scheme to come up with a two dimensional drive for powering a microplatform. Such an approach promises to fill industrial needs in the area of microassembly.

ACKNOWLEDGMENTS

The authors would like to thank A. Karyazin for precision grinding work dicing stators and travelers and machining the bearing races, as well as H. Schmeding and M. Beck for their help in supporting the motor's electrical and mechanical characterization. Finally, the authors are indebted to Sumitomo Special Metals, Osaka, Japan and Vacuumschmelze, Hanau, Germany for providing material samples.

REFERENCES

[1] H.H. Gatzen, et al.: "A Novel Variable Reluctance Micromotor for Linear Actuation", Proc. Actuator 2000, Bremen, pp. 363-366, 2000

[2] M. Madou, „Fundamentals of Microfabrication", CRC Press, Boca Raton 1997

[3] J. J. Sniegowski, et al.: "Monolithic Gear-Mechanisms Drive by a Polysilicon Surface-Micromachined On-Chip Electrostatic Micromachine" Solid State Sensor and Actuautor Workshop, Hilton Head Is., South Carolina, 1996, pp. 178-182

[4] E.J. O'Sullivan, et al.: "Integrated, Variable-Reluctance Magnetic Minimotor", IBM Journal of Research and Development Electrochemical Microfabrication Vol. 42, No. 5, 1998, p. 681

[5] C.W. Chang, et al.: "A Magnetically Actuated Scanner for Intravascular Ultrasound Imaging", Proceedings of the 2001 ASME International Mechanical Engineering Congress & Exposition, New York, November 11-16, 2001, Vol. 2, MEMS 23914

[6] B. Krevet, et al.. "A Miniaturized Laser Scanner in LIGA technology (MILS)", Proc. Actuator 2002, Bremen, pp. 312-315, 2002

[7] B. Wagner, et al.: "Permanent Magnet Micromotors on Silicon Substrates", Journal of Microelectromechanical Systems, Vol. 2, No. 1, pp. 23-29, 1993

[8] I. Boldea, S. A. Nasar: "Linear Electric Actuators and Generators", Cambrigde University Press, Cambridge, UK, 1997

[9] H.H. Gatzen, et al.: "High Precision Machining of a Longitudinal Bearing for a Linear Microactuator", 3rd Int. euspen conf., Eindhoven, The Netherlands, pp. 325-328, 2002

[10] M. Föhse, et al.: "Design, Fabrication, and Characterization of a Miniature Linear Asynchronous Motor", Proc. Actuator 2002, Bremen, pp. 176-179, 2002

[11] C. Kourouklis, et al.: "The Application of Chemical-Mechanical Polishing for Planarizing a SU-8/Permalloy Combination Used in MEMS Devices", Proc. EMSA 2002, Athens, Greece, (in press)

[12] T. Kohlmeier, et al.: "Application of UV Depth Lithography and 3D-Microforming for High Aspect Ratio Electromagnetic Microactuator Components", Microsystem Technologies, Vol. 8 (2002), pp. 304-307

[13] M. Föhse, et al.: "Investigations on the Pole Geometry Optimization of a Variable Reluctance Microactuator" 47. Internationales Wissenschaftliches Kolloqium, Ilmenau, 2002, pp. 215-216

[14] H.H. Gatzen, M. Beck: "Tribological Investigation of Micromachined Silicon Sliders", Tribology International, 2003 (in press)

[15] T. Budde, H.H. Gatzen: "Magnetic Properties of Thick Sputter Deposited SmCo Films For Mems-Applications", Digest Intermag Europe 2002, Amsterdam, The Netherlands, GD05 (submitted to J. of Magnetism and Magn. Mat.)